Analytical Methods

Accepted Manuscript

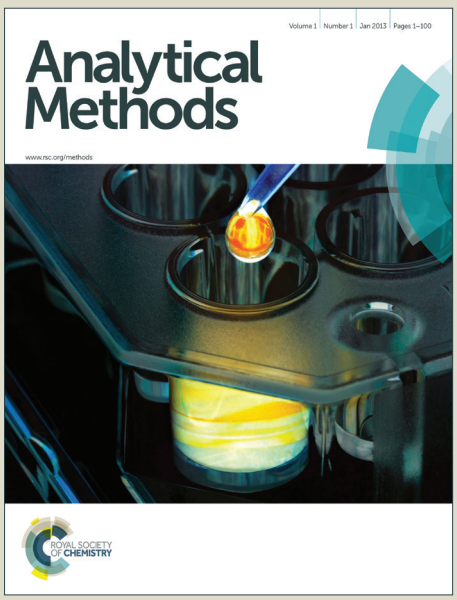

ROYAL SOCIETY OF CHEMISTRY

www.rsc.org/methods

Room-Temperature Phosphorescence of Biocompatible B_2O_3/SiO_2 Nanocomposite and their application for cellular imaging

Zhenjing Zhuang[1], Junping Zhang[1], Manman Zhang[1], Dan Xiao[2*]

[1] *Institute of Molecular Medicine, Huaqiao University, Fujian 362021, P.R. China.*

[2] *College of Chemistry, Sichuan University, Chengdu 610065, P.R. China.*

Abstract

A highly emissive broadband phosphor based on B_2O_3/SiO_2 nanoparticles was prepared using a sol-gel method. The room-temperature phosphorescence (RTP) produced from this phosphor was carefully studied and its phosphorescence spectra was found to be featured with two peaks in the visible region. One of the peak at 540 nmoriginated from B_2O_3 and the other at 470 nm generated from SiO_2. The B_2O_3/SiO_2 nanoparticles is noncytotoxic and possesses remarkable environmental stability. Therefore, the B_2O_3/SiO_2 phosphor can serve as bioprobes for cellular imaging.

Keywords: phosphorescence, cellular imaging, nanoparticles, silica, boron

* Corresponding author. Tel: +86-28-85415029; fax: +86-28-85416029.
E-mail addresses: xiaodan@scu.edu.cn.

1. Introduction

Room-temperature phosphors have drawn much attention due to potential applications in display and lighting technologies.[1,2] Moreover, room-temperature phosphorescence (RTP) has been utilized for detection and sensing techniques.[3-9] Recently, room-temperature phosphors have been studied in a number of doped semiconductor systems. For example, modified Mn doped ZnS QDs have been synthesized and used as RTP sensors for sensor application.[3-5] Doped silicon dioxide has also been employed as phosphor powders for color display[10] Some of them have acted as RTP sensors for the trace analysis of chemical species, such as TiO_2/SiO_2, ZnO/SiO_2, and PbO/SiO_2.[6-9] However, the emissive centers used in SiO_2-based phosphors are typically metal element which is expensive or environmentally toxic metals such as rare earth elements, [12,13] Ti,[6-7] Zn,[8] Pb,[9] and so on. There have been only a few reports on the nonmetal-doped SiO_2 phosphorescence material. Green et al. fabricated highly emissive air-stable phosphors at low temperatures, and ascribed the luminescence of the SiO_2 to the defects of carbon impurity.[10] Zhao et al. reported the Room-temperature metal-activator-free phosphorescence from mesoporous silica, and the luminescence centers in the mesoporous silica can also be assigned to the carbon substitutions for the silicon atoms in the silica network.[14] Boron resembles closely with silicon due to diagonal relationship. Boron is a useful dopant in silica glass (borosilicate glass) to improve its optical and mechanical properties. To the best of our knowledge, however, room-temperature phosphorescence from the boron-doped silica has never been reported.

Luminescent nanomaterials have attracted tremendous interest in biological imaging due to its real time and high resolution characteristics. A wide range of fluorescent nanoparticles include quantum dots have been used to develop novel intracellular nanoprobes.[15-25] Among these materials, silica is the most frequently used substance to fabricate fluorescent

nanoparticles due to its desirable properties including nontoxicity and biocompatibility.[19-25] For example, dye doped silica nanoparticles improve performance compared to the isolated dye molecules, such as intense fluorescence signal, minimized photobleaching, simple surface modification, and low toxicity etc.[19-22] Semiconductor QDs deposited with a silica shell would be helpful to reduce cytotoxicity.[23-25] These fluorophore-doping methods, however, can be time-consuming and expensive, and are commonly associated with issues like high toxicity, increased particle size, and dye-leaking.

In this paper, highly emissive broadband phosphors of B_2O_3/SiO_2 nanoparticles were synthesized and used as optical probe for live cell imaging. The B_2O_3/SiO_2 nanoparticles possess strong room-temperature phosphorescence that is stable against environmental changes. In vivo toxicity studies also demonstrated their their favorable biocompatibility. The as-prepared boron-doped silica nanoparticles can be tracked in vitro, suggesting the great potential of this technology in biological imaging.

2. Experimental

Reagents

Tetraethoxysilane （TEOS） was purchased from Tianjin Chemicals (Tianjin, China). Boric acid, glycerol, isopropyl alcohol, and ammonium hydroxide were obtained from Chengdu Chemicals Reagent Ltd (Sichuan, China). H_2O_2, Na_2S, $ZnCl_2$, KCl, NaCl, KI, Na_3PO_4, Na_2HPO_4, NaH_2PO_4, NH_4Cl, Na_2SO_4, $NaNO_3$, $Na_2C_2O_4$, $NaNO_2$, NaOH, HCl, ethanol, methanol, formaldehyde, benzene, toluene, petroleum ether, acetone, phenol, nitrophenol, dichloromethane, and chloroform were purchased from Shanghai Jingchun Reagent Ltd (Shanghai, China). dimethyl sulfoxide (DMSO) were purchased from Sinopharm Chemical

Reagent Co., Ltd. Thiazolyl blue tetrazolium bromide (MTT, M5655) was purchased from Sigma-Aldrich Inc. (St. Louis, USA). LysoTracker Red DND-99 was purchased from Invitrogen (Karlsruhe, Germany). Roswell Park Memorial Institute 1640 medium (RPML-1640) and Fetal Bovine Serum (FBS) were purchased from Life Technology(USA). NCI-H446 cells were obtained from American Type Culture Collection (ATCC). All reagents were of analytical grade or above and used without further purification. Redistilled water was used for the fabrication of the B_2O_3/SiO_2 nanoparticles, and all experiments were operated at room temperature.

Preparation of the B_2O_3/SiO_2

The nanometer particles of B_2O_3/SiO_2 were prepared by the sol–gel route. In a typical procedure, boric acid was dissolved in the mix solution of glycerol and water (1/3, v/v). TEOS was added into the above mixed solution and stirred continuously for 12 hours. Then 10% ammonium hydroxide was injected drop by drop. The solution was stirred until a transparent sol formed and gelled at room temperature. The gel was allowed to age for 24 h. Finally, calcination was performed at 550 □ for 3 hours, and nanometer-sized B_2O_3/SiO_2 particles were obtained. The samples were ground into powder before use. For comparison, undoped silica was synthesized under the same conditions as that mentioned above and calcined at 550 □ for 3 hours.

Instrumentation

Phosphorescence measurements were performed at room temperature using a fluorescence-phosphorescence spectrophotometer (Hitachi, F-7000) when the spectrophotometer was set in the phosphorescence mode with chopper arrangement. The scan speed was 240 nm/min. The slit widths of excitation and emission were all 5 nm. The

photomultiplier tube (PMT) voltage was set at 700 V. Infrared (IR) spectra were performed on an infrared spectrophotometer (Nicolet, NEXUS, FT-IR 670) with KBr discs. The microstructure of the nanocomposite was characterized by scanning electron microscopy (SEM) (Hitachi, S-4800) and transmission electron microscopy (TEM) (JEOL, 2010). For TEM measure, the B_2O_3/SiO_2 nanocomposites were ground into powder carefully, dispersed in alcohol and sonicated for half an hour before use. The X-ray diffraction patterns of the materials were measured with an X-ray diffractometer (XRD) (Dandong Fuyuan instrument, DX-1000). A ZF5 UV lamp (Shanghai Jiapeng, China) was used for UV irradiation when taking the RTP photographs. The pH measurements were taken on an Orion 720+ combined pH glass electrode (Thermo Electron, USA).

MTT assay of cell viability.

Human small cell lung cancer cell line NCI-H446 was originated from ATCC. NCI-H446 cells were seeded in 96-well plates (1×10^4 cells per well, Nunc 96-well MicroWell plates) cultured in Roswell Park Memorial Institute 1640 (RPML-1640) medium at 37 °C in a humidified atmosphere containing 5% CO_2 for 12 hours. B_2O_3/SiO_2 nanoparticles were pre-dispersed with DMSO to obtain different concentrations and then added into the chambers to reach a final concentration ranging from 0.1 -100 ug/ml. After an incubation time of 24-48 h at 37 °C in a humidified atmosphere containing 5% CO_2. 3-(4,5-dimethylthiazol-2-yl) -2,5-diphenyltetrazolium bromide (MTT) was dissolved in DMSO. 20 μL of MTT (5 mg/mL) was added into each well and the cells were incubated for a further 4 hours. Then the medium in each well was removed carefully and replaced with 200 μL DMSO. The 96-well plates were shaken for 15 min to dissolve the formazan crystals completely. The formazan concentration was finally quantified using a spectrophotometer (Tecan, Infinite M200) by measuring the

absorbance at 490 nm with background correction at 630 nm. A linear relationship between cell number and optical density was established, thus allowing for accurate quantification of changes in the rate of cell proliferation. The morphology of the cells was observed with an inverted fluorescence microscope (Nikon, TE-2000U) before MTT was added.

Cellular imaging

Human small cell lung cancer cell line NCI-H446 was originated from ATCC. The cells were cultured in DMEM medium supplemented with 10% calf serum, 2.2 g/l $NaHCO_3$, 100 U/ml penicillin, and 100 g/ml streptomycin at 37 °C in a humidified atmosphere containing 5% CO_2.

To study the cellular uptake, 2×10^5 NCI-H446 cells were seeded in 20 mm glass bottom cell culture dish and cultured for 14 hours prior to the studies. B_2O_3/SiO_2 nanoparticles were added into the chambers to reach a final concentration of 10 μg/mL. The incubation was stopped after 24 h. The nanoparticles were removed, and the cells were rinsed 3 times with PBS (pH 7.4) and then fresh DMEM was added. The cells were imaged on Leica TCS-SP5 fluorescence microscope (leica, TCS-SP5). Excitation of the B_2O_3/SiO_2 nanoparticles was performed with a laser at λ= 405 nm, and emissions were collected using a wavelength range of 485–545 nm. For colocalization experiments, LysoTracker Red was added into the chambers after the nanoparticle solutions was removed, and cultured for 0.5 hour. Then the cells were rinsed 3 times with PBS (pH 7.4) and fresh DMEM was added.

3. Results and discussion

The nanometer particles of B_2O_3/SiO_2 were prepared by a sol-gel method according to the above-mentioned procedure. The phosphorescence intensities and experimental conditions are

summarized in Supporting Information Fig, S-1. When the B/Si molar ratio was 1:3 and the B_2O_3/SiO_2 was calcined at 550 ℃ for 3 h, the maximum phosphorescence intensity of B_2O_3/SiO_2 was obtained. If the calcination temperature exceeds 750 ℃, the room temperature phosphorescence of B_2O_3/SiO_2 composite oxides become very weak.

The morphological and composition of the obtained materials were carried out by SEM, TEM, FTIR, and XRD. The SEM and TEM images (Fig. 1A and B) show that the B_2O_3/SiO_2 nanoparticles have a wide size distribution due to aggregation. The diameter of particles was estimated to be between 20 and 30 nm. The XRD of the as-prepared phosphors are shown in Fig.2A. The wide angle XRD patterns show only the diffraction peak of non-crystalline silica frameworks for undoped silica, and three weak peaks have been observed in the B_2O_3/SiO_2 nanocomposite. The weak characteristic peaks are consistent with the standard diffraction patterns (JCPDS Card No. 13-0420) and belong to B_2O_3. This result demonstrates that there are B_2O_3 in the SiO_2 matrix. To show the reaction-induced chemical bonding, FTIR spectra of the as-prepared B_2O_3/SiO_2 nanoparticles were measured (Fig. 2B), which feature several distinct absorption peaks in the range of 1000−3500 cm^{-1}. Typically, the absorptions in 1500 - 1300 cm^{-1} and 3200 cm^{-1} are assigned to stretching vibrations of B-O-B and BO-H respectively. this results further demonstrate that there are B_2O_3 in B_2O_3/SiO_2 phosphors. Additional, the IR band observed at 930 - 915 cm^{-1} and 675 cm^{-1} are widely accepted as the characteristic vibration due to the formation of B-O-Si bonds.[26] This indicates that B substitutes for Si, which is assumed to form the trap levels. This results in the broadband phosphorescence.

Ultraviolet excitation of the B_2O_3/SiO_2 nanocomposite sample resulted in strong luminescent, and more interestingly, the emission can persist for several seconds after the excitation light is switched off. Such a long lifetime classifies the light emission as

phosphorescence. Insert in Fig. 3 shows the phosphorescence photographs of the typical B_2O_3/SiO_2 nanocomposite sample in a powder under excitation at 365 nm. Strong green emission was visualized even by the naked eye after the excitation light is switched off.

The luminescence of the SiO_2 is well-known and has been ascribed to the defects (such as oxygen vacancy, carbon impurity).[27,10] The structure defects of the sol-gel SiO_2 can be affected by the mental oxide impurity of TiO_2, PbO, and ZnO.[6-9] In order to understand the mechanisms of RTP for boron-doped silica, we characterized the phosphorescence properties of the B_2O_3/SiO_2 nanocomposite and pure silica in detail. Fig. 3 shows the excitation and emission spectra of B_2O_3/SiO_2 nanocomposite and pure silica. The relative phosphorescence intensity of B_2O_3/SiO_2 nanocomposite increases remarkably than that of the pure SiO_2. The B_2O_3/SiO_2 nanocomposite exhibits two peaks around 470 nm and 540 nm, but only a peak at around 470 nm was observed in the spectrum of the pure silica when excited at 370 nm. Therefore, we suppose that the emission band peaking at about 470 nm originates from the SiO_2 while the emission peak at 540 nm originates from the defects of B_2O_3. To confirm such a supposition we studied the excitation spectrum of as-prepared SiO_2 by emission at a wavelength of 470 nm and 540 nm, respectively. As shown in Fig. 3B, the excitation spectra of B_2O_3/SiO_2 nanocomposite display two peaks at around 370 nm and 430 nm when monitored at 540 nm and and four peaks at about 295 nm, 330 nm, 370 nm and 435 nm when monitored at 470 nm. Pure silica display two peaks at about 290 and 330 nm when they are monitored at 470 nm. It is clear that the location of the excitation peak at about 295 nm and 330 nm, for B_2O_3/SiO_2 nanocomposite is similar with which for pure silica. Furthermore, the emission spectrum for B_2O_3/SiO_2 nanocomposite shows only one peak at about 470 nm upon excitation at 295 nm. It can thus be deduced that the structure defects of the sol-gel SiO_2 can be affected by the impurity of B_2O_3 and the B_2O_3/SiO_2

phosphor is mainly due to the interaction between B_2O_3 and SiO_2. In the phosphorescence spectra of B_2O_3/SiO_2 nanocomposite, the emission peak at around 470 nm is ascribed to the defect luminescence in the SiO_2; and the emission peak at around 540 nm is ascribed to the centers involving B_2O_3. Moreover, the excitation spectra shown in Fig. 3 (cure a and b) indicate that the B_2O_3/SiO_2 nanocomposite can be efficiently excited at wavelengths ranging from 300 to 500 nm. The strong luminescence and broad excitation window allow us to excite the B_2O_3/SiO_2 nanocomposite with different ultraviolet light sources, such as HeCd lasers, Xe lamps, and hand-held ultraviolet lamps. Phosphorescence lifetime was measured with employing a Hitachi FL-7000 instrument. The exaction wavelength was at 370 nm. The decay curves of B_2O_3/SiO_2 nanocomposite are shown in Fig. 4. The life times are all about 3 s for phosphorescence emission at 540 nm (dash curve) and 470 nm (solid curve). These lifetimes are much longer than the fluorescence lifetimes of organic dyes and semiconductor QDs, which are typically on the order of nanoseconds and 10–40 ns respectively.

In our previously work, H_2O_2 and S^{2-} sensors were fabricated because the phosphorescence of TiO_2/SiO_2 can be quenched by H_2O_2,[6,7] and the phosphorescence of PbO/SiO_2 and ZnO/SiO_2 can be quenched by S^{2-},[8-9] respectively. However, in this work, the phosphorescence from the B_2O_3/SiO_2 nanoparticles is very stable against environmental changes. As shown in Fig. 5, the phosphorescence intensity remains constant in acidic-to-basic environments spanning a pH range of 0-12. It is note that the phosphorescence intensity keep constant after mixed B_2O_3/SiO_2 nanocomposite and 1 $mol \cdot L^{-1}$ HCl for 12 hours. However, the phosphorescence intensity dropped sharply when the pH above 12.0, it may be due to the B_2O_3/SiO_2 nanocomposite reaction with alkali.[8] In fact, we found B_2O_3/SiO_2 nanocomposite disappeared after interaction with 1 $mol \cdot L^{-1}$ NaOH and the phosphorescence was vanished.

Furthermore, the phosphorescence cannot be quenched when the B_2O_3/SiO_2 nanoparticles is in 1 mol·L^{-1} the following substances as H_2O_2, S^{2-}, Na^+, K^+, Zn^{2+}, Cl^-, I^-, PO_4^{3-}, HPO_4^{2-}, $H_2PO_4^-$, NH_3^-, NH_4^+, SO_4^{2-}, NO_3^-, $C_2O_4^{2-}$, NO_2^-. Organic molecules, such as ethanol, methanol, formaldehyde, benzene, toluene, petroleum ether, acetone, phenol, nitrophenol, dichloromethane, and chloroform, did not affect the phosphorescence intensity of B_2O_3/SiO_2 nanoparticles.

The remarkable environmental stability of luminescent property makes them attractive for biomedical application. Prior to the application of B_2O_3/SiO_2 nanoparticles as a cellular labeling agent, it is important to assess the potential cytotoxicity of B_2O_3/SiO_2 nanoparticles. In this study, Human small cell lung cancer cell line NCI-H446, originated from ATCC, was chosen for cytotoxicity evaluation by using an MTT assay. The result is presented in Fig. 6 A, it can be seen that there is no appreciable cytotoxicity to the NCI-H446 cells after being cultured with B_2O_3/SiO_2 nanoparticles for 48 h with B_2O_3/SiO_2 nanoparticles concentrations up 0.1 to 100 μg·mL^{-1}. The result suggests that the synthesized B_2O_3/SiO_2 nanoparticles are feeble cytotoxicity and suitable for biomedical applications. Microscopic studies confirmed the biochemical assays of cellular viability. As shown in Figure 6B, no obvious morphological change of NCI-H446 cells was observed in the presence of B_2O_3/SiO_2 nanoparticles after incubation for 48 h. These data suggest noncytotoxic of the B_2O_3/SiO_2 nanoparticles to the cells.

In the cellular uptake process, the exogenous particles are enclosed into endosomes initially, which mature into late endosomes or multivesicular bodies and eventually fuse with lysosomes.[28] To track the B_2O_3/SiO_2 nanoparticles following their uptake, the lysosomal compartment of the cultured cells was stained with the LysoTracker Red probe. The

LysoTracker Red are fluorescent acidotropic probes for labeling and tracking acidic organelles in live cells, primarily lysosomes with high selectivity and effective labeling of living cells at nanomolar concentrations.[29] When the lysosomes are stained (Figure 7B, red) a colocalization of the B_2O_3/SiO_2 nanoparticles (Figure 7A, green) can be observed with laser-scanning confocal fluorescent microscopy, which is shown by the overlay of both fluorescence intensities (Figure 7C, yellow). The B_2O_3/SiO_2 nanoparticles (green) mostly overlap with the red staining indicating lysosomal localization (yellow), suggesting that B_2O_3/SiO_2 nanoparticles preferentially localize to the lysosomal compartment. It should be note that the images were obtained from laser-scanning confocal fluorescent microscopy set in the fluorescence mode with the fluorescence signals employed. The result demonstrates that B_2O_3/SiO_2 nanoparticles could serve as a better probe for further exploring phosphorescence-based applications in biomedical.

4. Conclusion

We prepared and characterized room-temperature phosphorescence from B_2O_3/SiO_2 nanoparticles. The luminescence emission is very strong and can persist for seconds after the excitation light is switched off. The emission band centered at 540 nm originates from B_2O_3 while that centered at 470 nm originates from SiO_2. Significantly, the luminescence from the B_2O_3/SiO_2 nanoparticles is low cytotoxicity and possessed remarkable environmental stability. Application of B_2O_3/SiO_2 nanoparticles in vitro image was also demonstrated. B_2O_3/SiO_2 nanoparticles can be uptaken by cells, presumably through endocytosis, resulting in high lysosomal selectivity as demonstrated through colocalization experiments with Lysotracker Red. The specificity of our probe suggests a strategy to overcome limitations for currently used

lysosomal fluorescent trackers by phosphorescence-based applications of B_2O_3/SiO_2 nanoparticles. Furthermore, these new biomaterials may be further conjugated with other biomolecules, such as antibody, peptides, and aptamer, hence providing a unique platform for target imaging of other biological systems.

Acknowledgements

This work was supported by Natural Science foundation of Fujian Province,China (No. 2010J05026) and National Natural Science foundation of China (No. 21307034)

Reference

1 M. A. Baldo, D. F. O'Brien, Y. You, A. Shoustikov, S. Sibley, M. E. Thompson amd S. R. Forrest, *Nature,* 1998, **395**, 151.

2 D. Le, O. Bolton, B. C. Kim, J. H. Youk, S. Takayama and J. Kim. *J. Am. Chem. Soc.*, 2013, **135**, 6325.

3 P. Wu, Y. He, H.-F. Wang and X.-P. Yan. *Anal. Chem.*, 2010, **82**, 1427.

4 W. Y. Xie, W. T. Huang, H. Q. Luo and N. B. Li, *Analyst*, 2012, **137**, 4651.

5 L. Dan and H.-F. Wang, *Anal. Chem.*, 2013, **85**, 4844.

6 X. Shu, Y. Chen, H. Yuan, S. Gao and D. Xiao, *Anal. Chem.*, 2007, **79**, 3695.

7 Y.Li, X. Y.Liu, H. Y.Yuan and D. Xiao, *Biosens. Bioelectron.*, 2009, **24**, 3706.

8 T. Zhou, N. Wang, C. Li, H. Yuan and D. Xiao, *Anal. Chem.*, 2013, 8, 1705.

9 N. Wang, T. Zhou, J. Wang, H. Yuan and D. Xiao, *Analyst*, 2010, **135,** 2386..

10 W. H. Green, K. P. Le, J. Grey, T. T. Au and M. J. Sailor, *Science*, 1997, **276**, 1826.

11 L. Zhao, T. Ming, H. Chen, L. Gong, J. Chen and J. Wang. *Phys. Chem. Chem. Phys.*, 2011, **13**, 2387.

12 E. Danielson, M. Devenney, D. M. Giaquinta, J. H. Golden, R. C. Haushalter, E. W. McFarland, D. M. Poojary, C. M. Reaves, W. H. Weinberg and X. D. Wu, *Science*, 1998, **279**, 837.

13 M. Yu, J. Lin, Z. Wang, J. Fu, S. Wang, H. J. Zhang and Y. C. Han, *Chem. Mater.*, 2002, **14**,

2224.

14 X. Hao, M. Zhou, X. Zhang, J. Yu, J. Jie, C Yu and X. Zhang, *Chem. Comm.*, 2014, **50**, 737.

15 Y. Zhong, F. Peng, F. Bao, S. Wang, X. Ji, L. Yang, Y. Su, S.-T. Lee and Y. He, *J. Am. Chem. Soc.*, 2013, **135**, 8350.

16 X. Diao, W Li, J. Yu, X. Wang, X. Zhang, Y. Yang, F. An, Z. Liu and X. Zhang. *Nanoscale*, 2012, **4**, 5373.

17 W. Sun, J. Yu, R. Deng, Y. Rong, B. Fujimoto, C. Wu, H. Zhang and D. T. Chiu. *Angew. Chem. Int. Ed.*, 2013, 52, 11294.

18 A. R. Maity, S. Palmal, S. K. Basiruddin, N. S. Karan, S Sarkar, N. Pradhan and N R. Jana. *Nanoscale*, 2013, **5**, 5506.

19 Z. Cai, Z. Ye, X. Yang, Y. Chang, H. Wang and Y. Liu *Nanoscale*, 2011, **3**, 1974.

20 S. Chen, Y. Yang, H. Li, X. Zhou and M. Liu. *Chem. Commun.*, 2014, **50**, 283.

21 J. Geng, J. Liu, J. Liang, H. Shi and B. Liu, *Nanoscale*, 2013, **5**, 8593.

22 X. Hong, Z. Wang, J. Yang, Q. Zheng, S. Zong, Y. Sheng, D. Zhu, C. Tang and Y Cui, *Analyst*, 2012, **137**, 4140.

23 L. Deng, L. Liu, C. Zhu, D. Li and S. Dong, *Chem Commun (Camb)*., 2013, **49**, 2503.

24 S. Veeranarayanan, A. C. Poulose, M. S. Mohamed, Y. Nagaoka, S. Iwai, Y. Nakagame, S. Kashiwada, Y. Yoshida, T. Maekawa and D. S. Kumar, *Int J Nanomedicine*., 2012, **7**, 3769.

25 M. Rahman, M. Z. Ahmad, I. Kazmi, S. Akhter, M. Afzal, G. Gupta and V. R. Sinha. *Curr Drug Discov Technol*., 2012, **9**, 319.

26 G. D. Sorarù, N. Dallabona, C. Gervais and F. Babonneau, *Chem. Mater.*, 1999, **11**, 910.

27 L. Vaccaro, A. Morana, V. Radzig and M. Cannas, *J. Phys. Chem. C*, 2011, **115**, 19476.

28 A.-R. Marco, S. Diabaté and C. Weiss, *Arch. Toxicol.*, 2011, 85, 813.

29 H. M. Kim, M. J. An, J. H. Hong, B. H. Jeong, O. Kwon, J.-Y. Hyon, S.-C. Hong, K. J. Lee and B. R. Cho, *Angew. Chem.*, 2008, **120,** 2263.

Figure captions

Fig. 1 SEM (A) and TEM (B) image of B_2O_3/SiO_2 nanocomposite. Scale bars: 500 nm and 200 nm, respectively.

Fig. 2 XRD patterns (A) and FTIR spectra (B) of the obtained silica sample. Cure a is pure silica sample and cure b is B_2O_3/SiO_2 nanocomposite.

Fig. 3 Room temperature phosphorescence excitation and emission spectrum of the sample when the calcination was performed at 550□ for 3 hour. Curve a and b are phosphorescence excitation spectrum of B_2O_3/SiO_2 when emission at 470 nm and 540 nm respectively. Curve c and d are phosphorescence emission spectrum of B_2O_3/SiO_2 excited at 370 nm and 295 nm respectively. Curve e is phosphorescence excitation spectrum of undoped SiO_2 when emission at 470 nm. Curve f is phosphorescence emission spectrum of undoped SiO_2 excited at 330 nm. Insert is the phosphorescence photographs of the typical B_2O_3/SiO_2 nanocomposite sample in a powder after the excitation light at 365 nm is switched off.

Fig. 4 Phosphorescence intensity decay curves of B_2O_3/SiO_2 nanocomposite when excited at 370 nm.

Fig. 5 Phosphorescence stability of B_2O_3/SiO_2 nanocomposite at varying pH values.

Fig. 6 (A) Cell viability of NCI-H446 cells incubated with 0.1 - 100 $\mu g \cdot mL^{-1} B_2O_3/SiO_2$ nanocomposite for different time. The cell viability was calculated as a percentage from the viability of the control (untreated) cells. The viability of the control cells was considered 100%. The results are means ± SD from three impendent experiments. (B) Microscopic imaging of NCI-H446 cells after incubated with B_2O_3/SiO_2 nanoparticles for 48 h.

Fig. 7 Fluorescence microscopy imaging of NCI-H446 cells by confocal laser scanning fluorescence microscopy. (A) Cells were treated with B_2O_3/SiO_2 nanoparticles for 24 h. (B) Cells treated with B_2O_3/SiO_2 nanoparticles for 24 h were stained with LysoTracker Red. (C) overlapped image of (A) and (B).

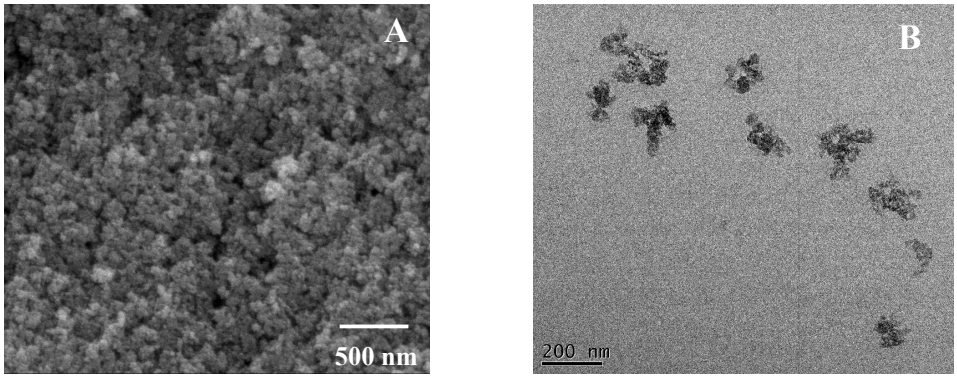

Fig. 1 SEM (A) and TEM (B) image of B_2O_3/SiO_2 nanocomposite. Scale bars: 500 nm and 200 nm, respectively

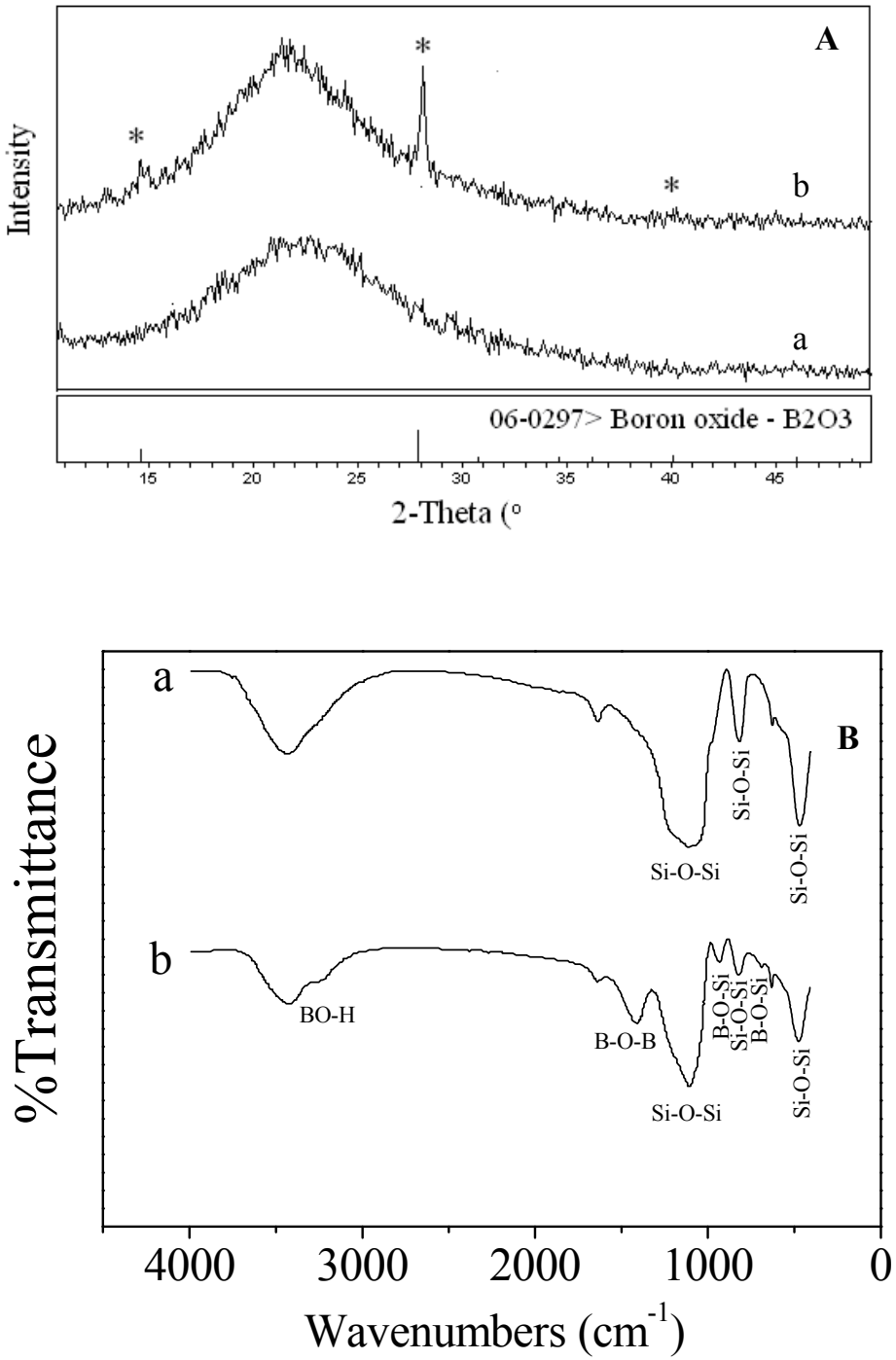

Fig. 2 XRD patterns (A) and FTIR spectra (B) of the obtained silica sample. (curve a) pure silica sample; (curve b) B_2O_3/SiO_2 nanocomposite.

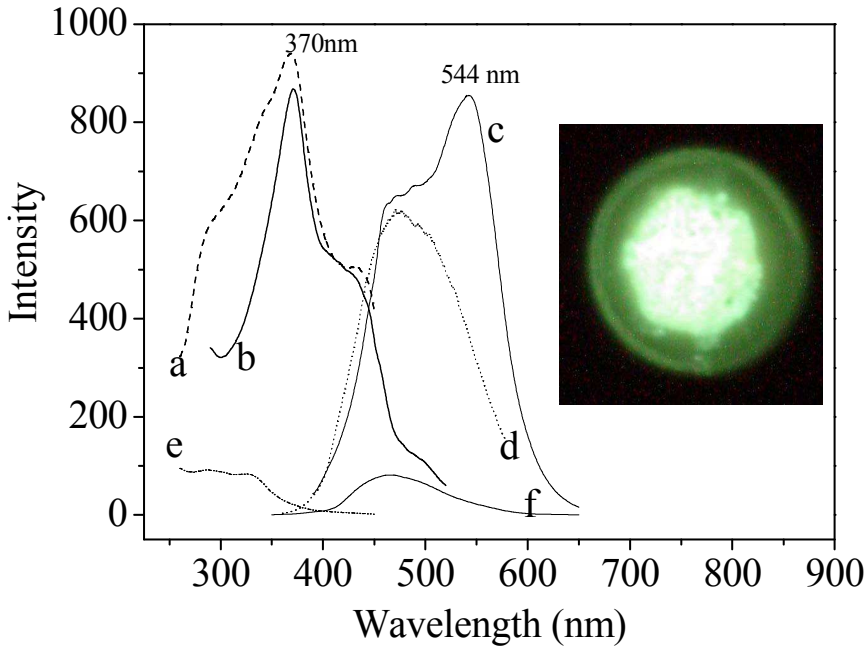

Fig. 3 Room temperature phosphorescence excitation and emission spectrum of the sample when the calcination was performed at 550□ for 3 hour. Curve a and b are phosphorescence excitation spectrum of B_2O_3/SiO_2 when emission at 470 nm and 540 nm respectively. Curve c and d are phosphorescence emission spectrum of B_2O_3/SiO_2 excited at 370 nm and 295 nm respectively. Curve e is phosphorescence excitation spectrum of undoped SiO_2 when emission at 470 nm. Curve f is phosphorescence emission spectrum of undoped SiO_2 excited at 330 nm. Insert is the phosphorescence photographs of the typical B_2O_3/SiO_2 nanocomposite sample in a powder after the excitation light at 365 nm is switched off.

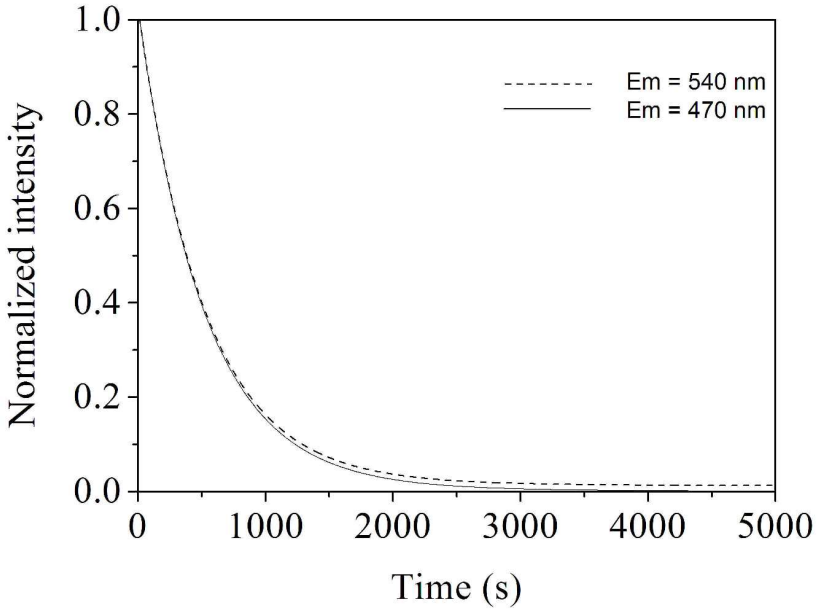

Fig. 4 Phosphorescence intensity decay curves of B_2O_3/SiO_2 nanocomposite when excited at 370 nm.

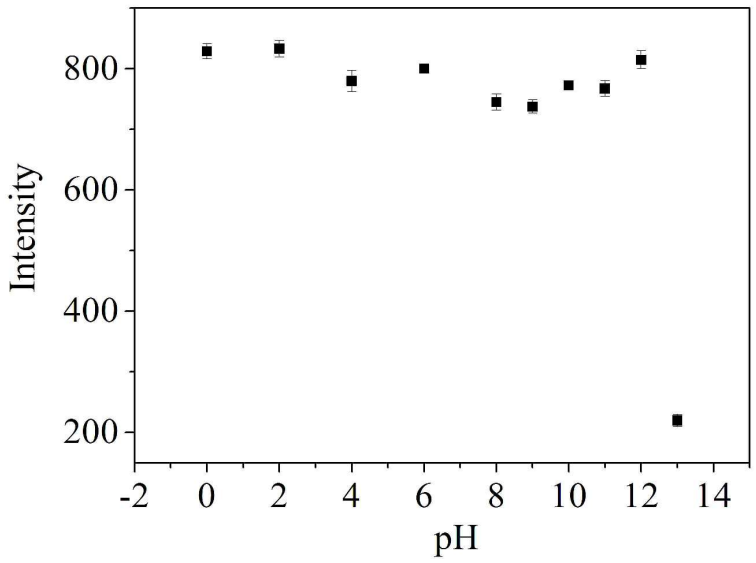

Fig. 5 Phosphorescence stability of B_2O_3/SiO_2 nanocomposite at varying pH values.

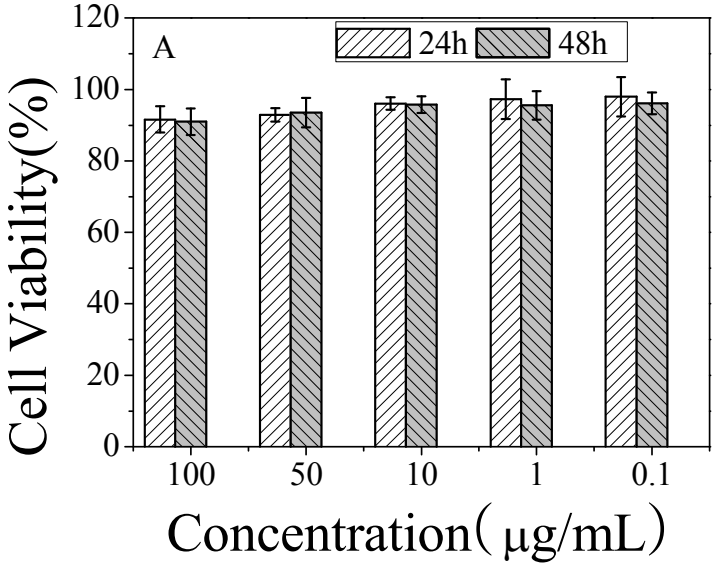

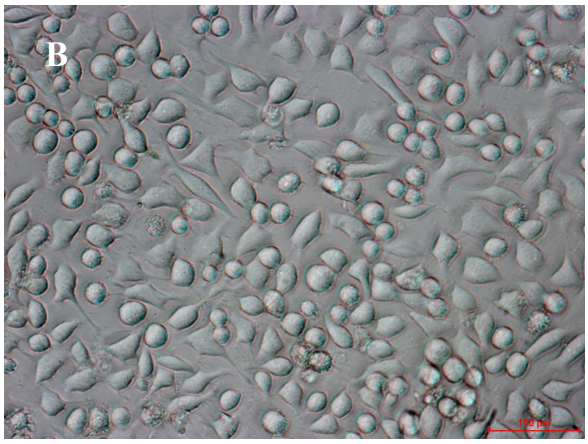

Fig. 6 (A) Cell viability of NCI-H446 cells incubated with 0.1 - 100 μg·mL^{-1} B_2O_3/SiO_2 nanocomposite for different time. The cell viability was calculated as a percentage from the viability of the control (untreated) cells. The viability of the control cells was considered 100%. The results are means ± SD from three impendent experiments. (B) Microscopic imaging of NCI-H446 cells after incubated with B_2O_3/SiO_2 nanoparticles for 48 h. Scale bars: 100 nm.

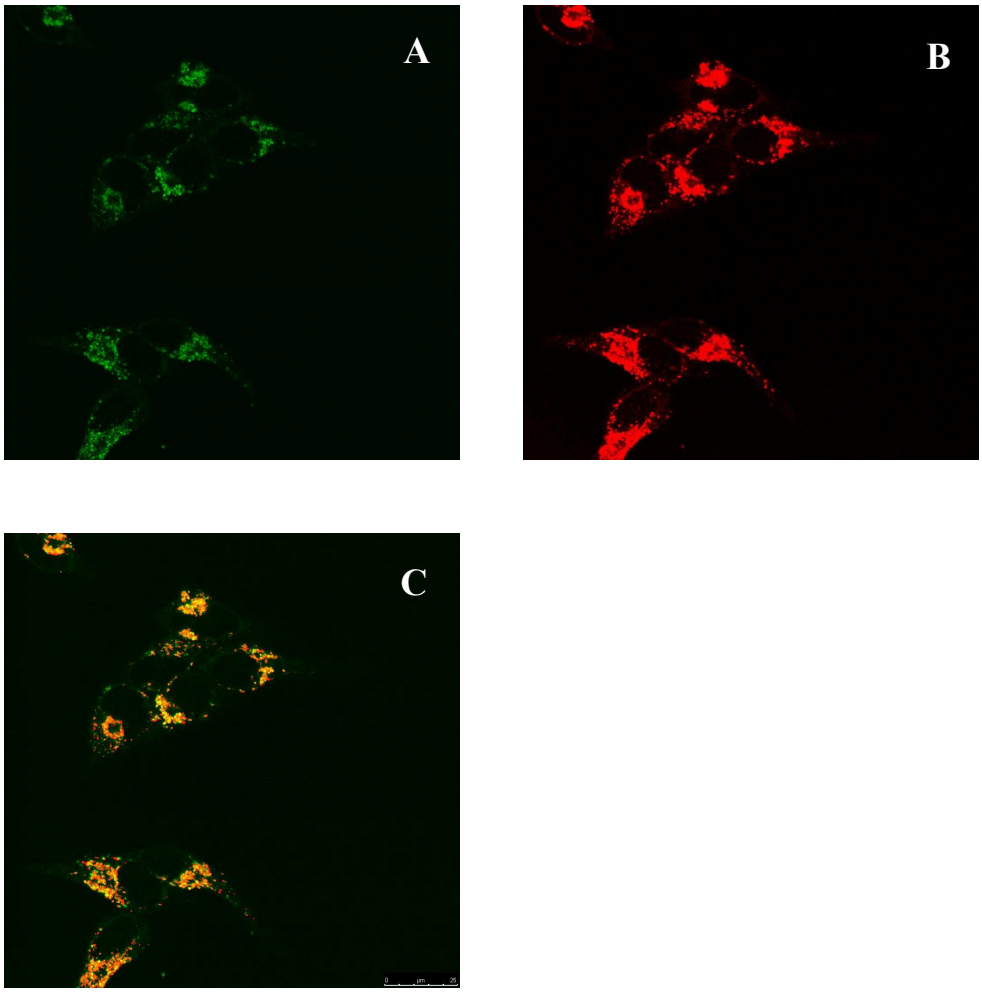

Fig. 7 Fluorescence microscopy imaging of NCI-H446 cells by confocal laser scanning fluorescence microscopy. (A) Cells were treated with B_2O_3/SiO_2 nanoparticles for 24 h. (B) Cells treated with B_2O_3/SiO_2 nanoparticles for 24 h were stained with LysoTracker Red. (C) overlapped image of (A) and (B).